Ninth International Conference on CFD in the Minerals and Process Industries
CSIRO, Melbourne, Australia
10-12 December 2012

EXPERIMENTAL VALIDATION AND INDUSTRIAL APPLICATION OF A NOVEL NUMERICAL MODEL FOR CONTINUOUS CASTING OF STEEL

Pavel E. RAMIREZ LOPEZ[1*], Johan, BJÖRKVALL[1], Ulf SJÖSTRÖM[1], Peter D. LEE[2], Kenneth C. MILLS[3], Björn JÖNSSON[4], Jesper JANIS[4], Marko PETÄJÄJÄRVI[4] and Jarno PIRINEN[5]

[1] Casting and Flow Simulation Group, Swerea MEFOS
Aronstorpsvägen 1, SE 974 37 Luleå, SWEDEN

[2] School of Materials, The University of Manchester,
Rutherford Appleton Laboratory, Didcot, Oxon, OX11 OFA, UNITED KINGDOM

[3] Department of Materials, Imperial College London,
Prince Consort Road, SW7 2AZ, London, UNITED KINGDOM

[4] Outokumpu Stainless AB and Outokumpu Oyj,
Box 74 SE-77422 Avesta, SWEDEN and FIN-95490 Tornio, FINLAND

[5] Development Engineer, Continuous Casting,
Rautaruukki Oyj, Tervaraitti 4 B 26, 90100 Oulu, FINLAND

*Corresponding author: pavel.ramirez.lopez@mefos.se

ABSTRACT

Swerea MEFOS has worked intensively on the development of numerical models for Continuous Casting (CC) through a long list of projects co-funded by Scandinavian and other European steel producers in the past 25 years. More recently, MEFOS has accumulated critical mass regarding CFD, which made possible the development of a novel numerical model for the casting process. Its main feature is the prediction of slag infiltration (lubrication) as a result of adding the casting powder phase to simulations. This manuscript presents such modelling methodology in 2D and 3D, which is able to predict the metal/slag flow, heat transfer, solidification and mould oscillation within the CC mould. Validation is supported by plant trials and the recent revamping of an experimental metal model of industrial scale (Continuous Casting Simulator, CCS-1) able to replicate realistically the flow conditions in the caster.

BACKGROUND

Continuous Casting modelling has experienced profound changes since its incipient beginnings in the 1980's, where 1D (1-dimensional) models for heat transfer where the norm (Takeuchi *et al.*, 1985). With time, a series of milestones have been achieved, including the coupling of heat transfer to the turbulent metal flow within the mould (Huang *et al.*, 1998), modelling shell solidification (Thomas *et al.*, 1997), calculating the addition of argon as secondary phase to float inclusions (Pfeiler *et al.*, 2005), capturing the free surface or metal level (Anagnostopoulos *et al.*, 1999) and predicting the influence of Electro-Magnetics to stabilize the metal flow at high casting speeds (Kunstreich *et al.*, 2005). At the same time, the paradigm of uni-dimensionality was broken thanks to more powerful computers; as a result, 2D/3D dimensional models became widespread (Hasan *et al.*, 1998).

Nevertheless, to a large extent, these modelling efforts are focused on replicating the trends seen in the casters as well as predicting periods of "stable operation". For instance, most CC models predict the formation of the shell from heat flux curves obtained from statistics of several casters as exemplified by Figure **1** (Li *et al.*, 2002):

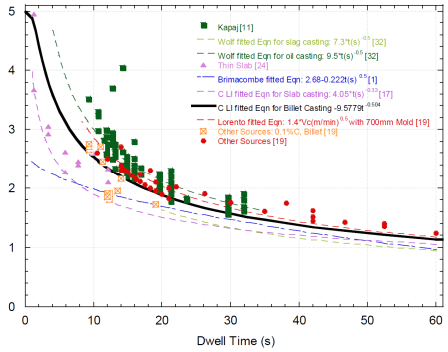

Figure 1: Typical heat flux fitting for heat transfer calculations, after (Li *et al.*, 2002).

As expected, the predicted mould temperatures and shell thickness from these models lie within normal limits of caster operation. However, specific caster characteristics such as nozzle design, mould size, casting speed, etc. are completely underestimated, since the casters used for the statistics are significantly different. Furthermore, heat transfer and solidification within the mould are deeply affected by the choice of steel grade, casting powder, mould oscillation, etc., which are completely ignored if a fixed heat flux or shell growth law is chosen as boundary condition for solidification. As a consequence, one of the main obstacles for complete adoption of modelling in the casting floor is its inability to predict the occurrence of specific problems or "singularities" such as breakouts, stickers and cracks, which arise from the particular machine and casting practices used by each producer.

Numerical and physical modelling provides a good alternative to diagnose problems as well as working as a benchmark to find optimal conditions for the process. The present manuscript describes numerical models able to analyze specific casting practices and address particular problems such as standing wave formation, lack of lubrication (powder consumption) and mould oscillation. Validation through direct measurements in the casters and physical models is also presented. In combination, these tools make possible a better understanding of the casting practice and open the door for enhancing the productivity of the CC machine.

NUMERICAL MODEL

MEFOS has developed several CC models in the past 25 years, but more recently it has abandoned the predefined heat fluxes approach to develop a *fully coupled model* able to include the casting powder/slag phase into the calculations (Ramirez-Lopez *et al.*, 2010; Ramirez Lopez *et al.*, 2010). The main feature of this model is the prediction of slag infiltration (lubrication) by means of an extremely fine mesh in the meniscus and slag film region (~25 μm for 2D and ~300 μm for 3D models), Figure 2.

The fluid model is based on the solution of the Navier-Stokes equations for compressible viscous flow coupled with the Volume of Fluid (VOF) method (Liow *et al.*, 2001), which is applied when the calculation of the interface between steel-slag or slag-air is required. Otherwise, the scheme is reduced to a typical single-phase Navier-Stokes approach. In this scheme, the effective density (ρ_{mix}) and viscosity (μ_{mix}) are given by:

$$\rho_{mix} = \alpha_p \rho_p + (1-\alpha_q)\rho_q \tag{1}$$

$$\mu_{mix} = \alpha_p \mu_p + (1-\alpha_q)\mu_q \tag{2}$$

Where (α) is the phase fraction and the subscripts (p) and (q) represent any of the two phases present in the cell (steel or slag). Thus, the continuity equation for the volume fraction can be derived as:

$$\frac{\partial}{\partial t}\left(\alpha_q \rho_q\right) + \nabla \cdot \left(\alpha_q \rho_q \vec{v}\right) = \sum_{p=1}^{n} \left(\dot{m}_{pq} - \dot{m}_{qp}\right) \tag{3}$$

where $\vec{v}$ is the overall velocity vector, $\dot{m}_{pq}$ is the mass transfer from phase p to phase q and $\dot{m}_{qp}$ is the opposite. The time discretization is then solved through an implicit scheme (FLUENT-User-Guide, 1995-2007):

$$\frac{\alpha_q^{n+1}\rho_q^{n+1} - \alpha_q^n \rho_q^n}{\Delta t} V + \sum_f \left(\rho_q^{n+1} U_f^{n+1} \alpha_{q,f}^{n+1}\right) = \left[\sum_{p=1}^{n}\left(\dot{m}_{pq} - \dot{m}_{qp}\right)\right] V \tag{4}$$

where V is the volume of the cell and U_f is the volume flux through the cell face. In a similar form, the VOF model solves a single set of momentum transfer equations for the velocity when two or more phases coexist in a calculation cell:

$$\frac{\partial}{\partial t}\left(\rho_{mix}\vec{v}\right) + \nabla \cdot \left(\rho_{mix}\vec{v}\vec{v}\right) = -\nabla P + \nabla \cdot \left[\mu_{mix}\left(\nabla \vec{v} + \nabla\left(-\frac{2}{3}\nabla \cdot \vec{v} I\right)\right)\right] + \rho_{mix}\vec{g} - S_s + S_\gamma \tag{5}$$

Where (P) is the pressure and ($\vec{g}$) is the gravitational force vector. The convective acceleration and the strain-rate tensor (second term left hand side and second term right hand side) are dependent on the volume fraction of all the phases through ρ_{mix} and μ_{mix} respectively. The last two terms are the momentum sink due to solidification and interfacial tension, respectively. S_γ is produced by the interfacial tension between steel-slag as calculated through the Continuum Surface Force model (Brackbill *et al.*, 1992) :

$$S_\gamma = \gamma_{p-q} \frac{\rho_{mix}\kappa_q \nabla \alpha_q}{\frac{1}{2}\left(\rho_p + \rho_q\right)} \tag{6}$$

where (γ_{p-q}) is the interfacial tension between steel and slag, while (κ_q) is the local surface curvature between any p and q phases (also defined by Brackbill). The velocity dampening due to turbulence (S_S) is calculated by:

$$S_s = \frac{\left(1-f_l\right)^2}{\left(0.001 + f_l^2\right)} A_{mush}\left(\vec{v} - v_c\right) \tag{7}$$

where A_{mush} is a constant, v_c is the casting speed and f_l is the liquid fraction of steel in the mushy zone as calculated by the lever rule method. Although such a simple solidification model and accompanied solidification constant A_{mush} are not fully able to capture the complex segregation behaviour of modern steel grades such as peritectics and Advanced High Strength Steels (AHSS); the predicted shell thicknesses are in good agreement with breakout samples and other works (Ramirez Lopez *et al.*, 2010). The authors are working actively in this topic through an RFCS (European Funded) project to describe more accurately the solidification behaviour of these steels through in-situ high temperature observations (Ramirez Lopez *et al.*, 2010).

Turbulence effects are calculated through the well known k-ε RNG model (Launder *et al.*, 1972), which can be activated or deactivated at will for the different regions in the numerical domain, including the shell and slag film.

Adding the casting powder/slag phase to the calculations allows explicit prediction of the slag film thickness. Therefore, the slag bed, rim and film are not predefined, and are result of the calculations. This makes possible to substitute the typical algebraic approach of heat resistances in the shell-mould gap by the effective resistance provided by the thermal properties of the slag:

$$r_{\text{int}} + \overbrace{\underbrace{\left(\frac{d_{cry}}{K_{cry}}\right) + \left(\frac{d_{glassy}}{K_{glassy}}\right)}_{solid-slag} + \underbrace{\left(\frac{d_{liquid}}{K_{liquid}}\right)}_{liquid-slag}}^{slag-film\ (r_{film})} = r_{\text{int}} + \overbrace{\frac{d_{film}}{K_{eff}}}^{r_{film}} \tag{8}$$

where the only resistance that is not possible to model is the interfacial resistance (r_{int}) produced by the rugosity of the solid slag in contact with the copper mould and is deduced from Equation (9):

$$r_{\text{int}} = 9 \times 10^{-5} \left(\text{CaO}/\text{SiO}_2\right)^{4.2} \tag{9}$$

Radiation is not included at this stage, but its effects are modelled by enhancing the slag thermal conductivity at high temperatures based on the fact that radiation accounts for only 15-20% of the heat removal at that temperature range. An example of typical boundary conditions and 2D/3D mesh used in the model are presented in Figure 2.

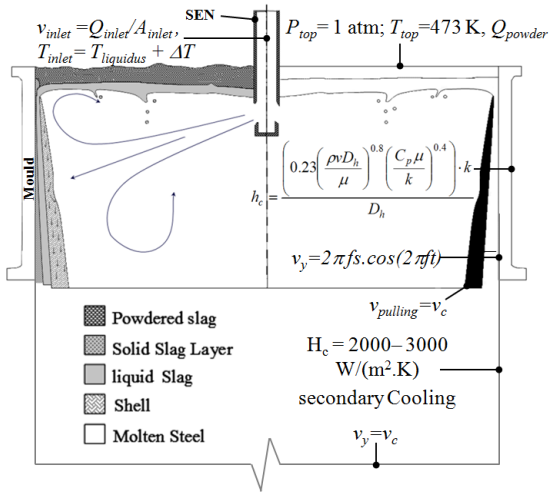

a)

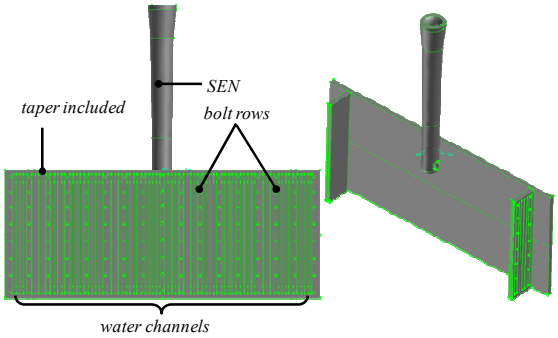

b)

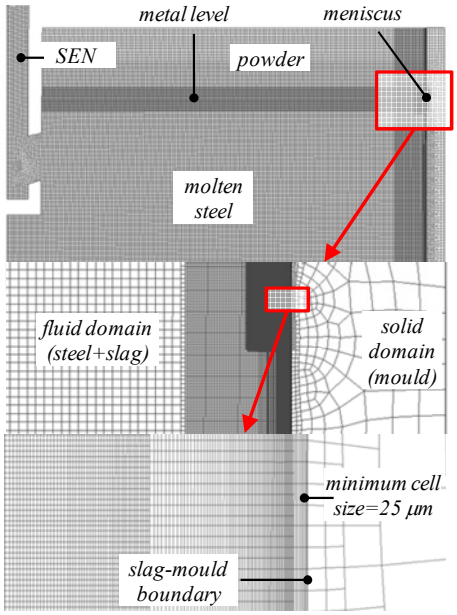

c)

Figure 2: Model setup, a) phases simulated and boundary conditions, b) mould assembly and c) detail of mesh used in the simulations.

PHYSICAL MODEL

Designed and built between 2004-2007 during a RFCS project (Higson *et al.*, 2010), the model is equivalent to a continuous casting system with tundish, stopper, Submerged Entry Nozzle (SEN) and mould as presented in Figure 3.

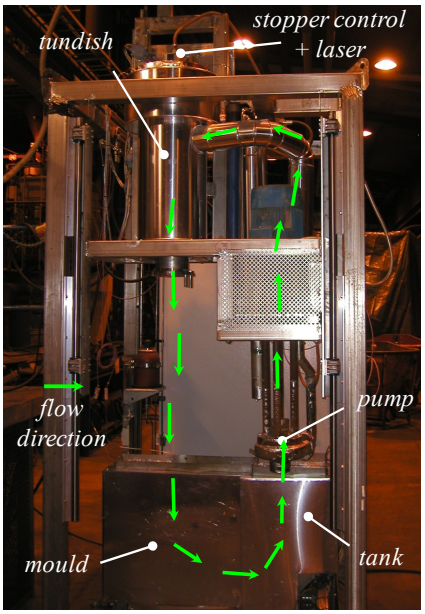

Figure 3: Continuous Casting Simulator, CCS-1.

The hot metal is transported continuously from the tundish to the mould, which is connected at the bottom to a tank/reservoir. This reservoir contains a submerged pump that sends the metal back to the tundish closing the flow loop. A low melting point alloy (137 °C) Bi-Sn, is used as working media to simulate the steel flow. Such alloy was chosen due to i) close resemblance of flow dynamic properties compared to steel and ii) non-toxicity. The properties of the alloy are presented in Table **1**, including its dynamic viscosity changes with temperature, which make it useful to model the behaviour of "sticky" grades (Figure **4**). The electrical properties of the alloy are also close to steel, which make it an ideal candidate for testing Electro Magnetic Stirring or Breaking devices.

Table 1: CCS-1 specifications and Bi-Sn alloy properties:

CCS-1 Specifications				
Mould size	0.8 x 0.2 x 0.9 m			
Tundish (metal holder)	h = 0.7-0.9 m			
Argon flow rate	Variable : up to 6 lt/min			
Immersion depth	Variable within 150 mm			
Bi-Sn alloy (MCP-137) properties compared to liquid steel				
	viscosity, μ (Pa-s x10^{-3})	density, ρ (kg/m³)	kinematic viscosity, ν (m²/s x10^{-6})	electrical conductivity, σ, (1/Ωm x10^6)
Steel (1600 C°)	6.3	7000	0.9	0.7
MCP 137 (150 C°)	10.7	8580	1.25	1.0
MCP 137 (170 C°)	8.6	8580	1	

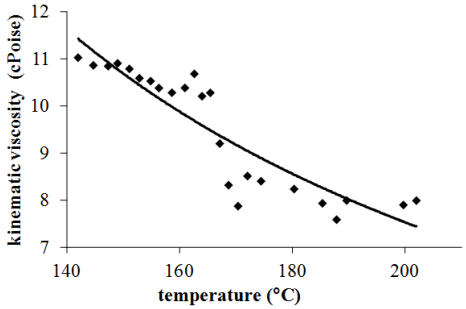

Figure 4: Kinematic viscosity of Bi-Sn alloy as a function of temperature.

The metal level in the tundish is controlled by a laser system within ~0.01 mm accuracy. Functionality tests have been performed with water, liquid metal and liquid metal+argon, while temperature can be controlled within ±1 °C during long trials (+6 hours) for casting speed ranges from 0.4 to 1.6 m/min (Figure **5**).

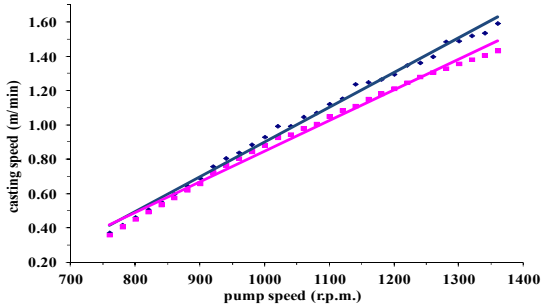

Figure 5: Pump speed vs casting speed for CCS-1

The model has been designed to use the same ceramic nozzles and stoppers as industrial casters or scaled stainless steel versions. A layer of 3-5 mm of high viscosity oil can be added to simulate the liquid slag pool behaviour in the real caster, while a video camera or mechanical sensors are used to analyse the metal flow. A variety of sensors to characterize the metal velocities have been tested in the model including: Ultrasonic Doppler Velocimetry, Electromagnetic Vives probe and a light beam sensor able to measure the metal level and oil layer thickness. A sample of these measurements is presented in the next section.

RESULTS SHOWCASE

The following results are an example of research projects performed for Scandinavian producers based on numerical modelling. However, validation activities including physical modelling and plant trials normally accompany the modelling activities. Simulation results were grouped into 3 main physical phenomena: Metal flow, heat transfer and solidification, while experiments and plant trials were used for validation when appropriate.

Metal Flow

Figure **6**-top presents the model predictions for a middle plane parallel to the wide faces, where typical flow structures can be identified. These include a discharging jet produced by the metal leaving the nozzle and entering the mould cavity and 2 areas of circulation known as upper and lower rolls. Ultrasound measurements were performed on a scaled nozzle (2:3) of similar design to corroborate this flow pattern obtaining good agreement (Figure **6**-bottom). The velocity measurements in liquid metal were performed via a transducer positioned at 18 immersion depths along 8 vertical lines between the nozzle port and the mould narrow face. The ultrasound measurements confirm the existence of the jet and upper roll structure seen in the simulations and known as "double roll" pattern (Dauby, 2011). This flow pattern is qualitatively well known in the industry; however, its flow velocities and effect on the metal level are less well understood. One of these effects is the formation of a *standing wave* created by the flow arising to the surface after hitting the narrow face. Direct measurements were conducted in-plant on a similar mould+SEN configuration with a nail board to analyse this standing wave and compare it with simulations on the same geometry.

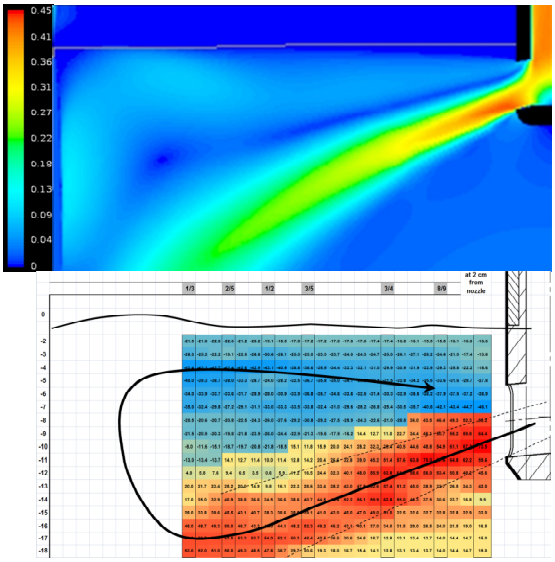

Figure 6: Flow pattern predictions vs ultrasound measurements for v_c=1 m/min

Figure **7** presents initially (top and middle) a comparison of the simulations in 2D and 3D to test the applicability of 2D models to simulate the system. Comparing the discharging jet angle, standing wave height and position shows that the 2D simulations are capable of capturing appropriately the flow pattern in the mould (Figure **7**, top).

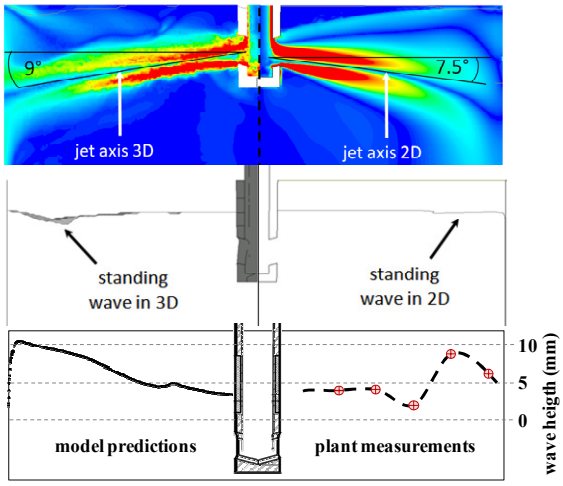

Figure 7: Predicted standing wave profile in 2D vs 3D vs plant measurements

The bottom of Figure **7** shows a comparison of the standing wave height and extension measured in the plant *versus* the slag-metal interface predicted in the simulations, achieving good agreement (Figure **8**).

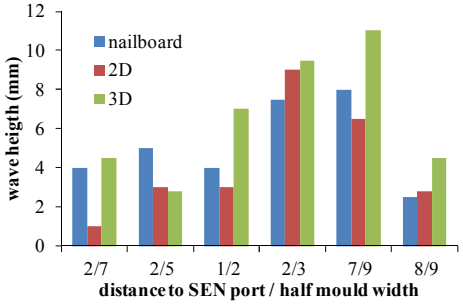

Figure 8: Predicted standing wave height in 2D vs 3D vs plant measurements.

Finally, the existence of a standing wave was also confirmed through the addition of oil at the surface of the liquid metal model to emulate the slag-pool behaviour. Figure **9** shows how the oil layer is pushed away from the narrow face due to the flow moving from the narrow face towards the nozzle (confirming also the *upper roll* flow pattern).

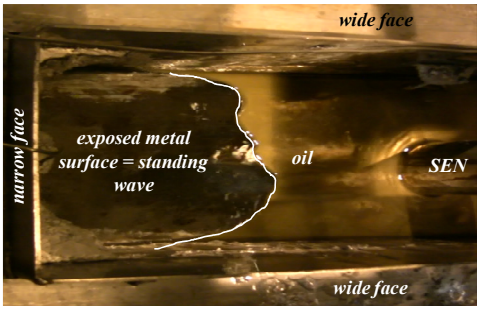

Figure 9: Oil layer simulating slag pool behaviour for v_c=1 m/min

Moreover, increasing the casting speed expands the area without slag cover, indicating a proportional increase of velocity at the interface and standing wave intensity (Figure **10**). Once the metal flow is validated for each particular caster configuration, a heat transfer analysis is carried out.

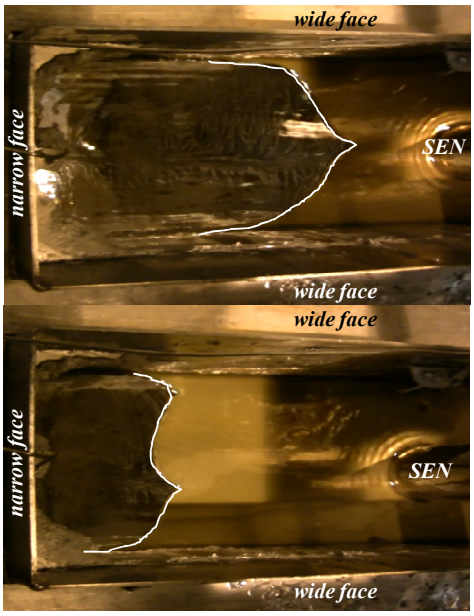

Figure 10: Oil layer simulating slag pool behaviour for v_c=1.4 m/min (top) and v_c=0.7 m/min (bottom).

Heat transfer

A point of interest regarding the influence of the metal flow on heat transfer was to analyse if the standing wave had a negative effect on lubrication. However, model predictions show that full infiltration is still possible and a smooth, round meniscus profile at the end of the standing wave is formed (Figure **11**a). The predicted temperature drop through the slag film from ~1050 °C (slab surface) to ~200 °C (mould surface) agrees well with the values seen in the plant (Figure **11**b). But more importantly, the total heat extracted is in agreement with the monitored increase of temperature in the mould cooling water as presented in Figure **11**c.

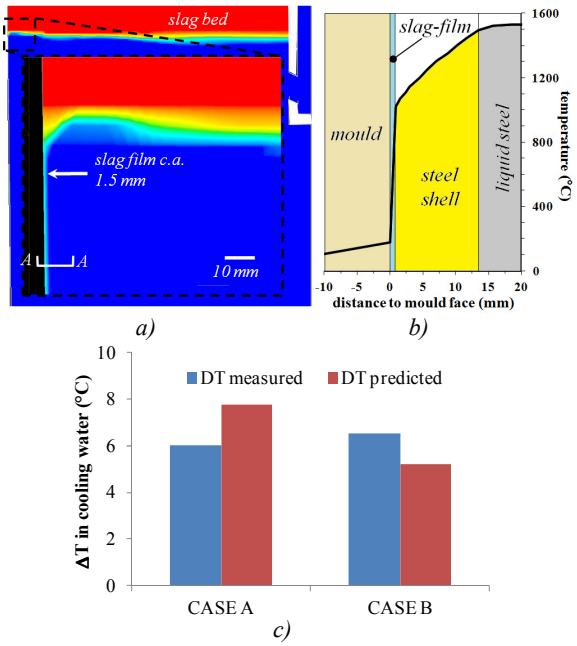

Figure 11: a) Slag film infiltration and resulting b) heat transfer in the shell-mould gap and c) ΔT in water *vs* plant measurements.

Solidification

As expected, heat transfer is closely related to shell growth since solidification is proportional to the overall heat flux removed through the mould. Figure **12** shows the predicted heat flux and shell growth evolution along the mould height for a time snapshot.

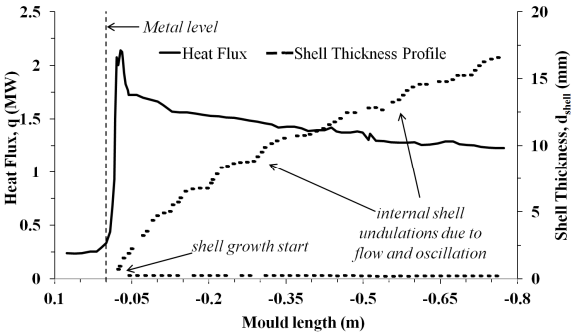

Figure 12: Heat flux and solidification *vs* mould length.

It is here where the particularities of each caster design and practices become evident; since rather than locating the peak heat flux at the metal level as most models, the peak occurs at least 30-50 mm below the metal level. This also gives an indication of where the meniscus curvature ends and the slag film begins. Interestingly, the tortuous internal shell shape predicted in the simulations bears more resemblance to actual measurements of shell breakouts (Santillana *et al.*, 2011). The shell is thin and weak during these first centimetres of solidification and any lack of lubrication at this position could lead to stickers or micro cracks, which under stress could turn into serious problems such as bleeders or even breakouts.

The importance of numerical modelling resides in its ability to predict the conditions leading to these particular events. However, the unsteady nature of the process makes difficult their identification through steady state models or statistical approaches like those mentioned earlier.

Even more, the coupling with metal flow dynamics is necessary for prediction of these problems, since most of them arise from fluctuations produced by the turbulent metal flow delivery to the mould. The transient approach used in the simulations together with small time steps (0.005 s) make possible the prediction of such fluctuations; and thereby, the changes on slag film thickness, heat flux and shell growth as a function of the metal flow and oscillation cycle as presented in Figure **13**.

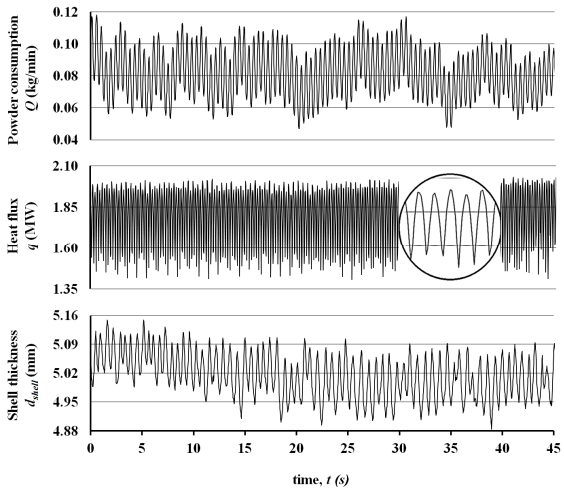

Figure 13: Typical model output showing data for powder consumption, heat flux and shell thickness measured in the mould side at 100 mm below the metal level.

CONCLUSIONS

A numerical model able to predict the multiphase (steel/slag) flow dynamics, heat transfer and solidification within the CC mould under transient conditions has been presented. The model has been used to analyse the casting practice of a variety of Scandinavian steelmakers on a series of projects, which included not only numerical simulations, but physical modelling and plant measurements. The physical modelling was carried out on a full scale liquid metal model based on a Bi-Sn alloy with low melting point (137°C). The following conclusions can be drawn from the industrial application of these models:

1. The numerical model is able to predict the metal flow within a CC mould including features such as jets and rolls. The existence of an upper roll as in the classic "*double-roll"* pattern was confirmed by ultrasound measurements and an oil layer over the metal surface (used as slag-pool simulator). The resulting standing wave formation was successfully predicted by the model as corroborated by physical models and plant measurements.
2. Despite the formation of a standing wave, the model was able to calculate the slag infiltration in the shell-mould gap as well as predicting accurately the heat removal through the mould, as validated with plant measurements. A fine mesh in the shell mould gap is necessary to capture accurately this heat removal and the extreme temperature gradients in the slag film.
3. The predicted shell formation starts 30-50 mm lower than the metal level and reveals a much more complex internal and external profile compared to statistical methods were a smooth parabolic shell shape is predicted. These profiles bear more resemblance with breakout samples seen in the industry.

The findings presented expose the dependency of flow dynamics, heat transfer and solidification on the particular characteristics of each caster (i.e. mould/nozzle design, casting practices, mould oscillation, etc). These should not be underestimated if realistic predictions need to be made. The transient calculation of heat transfer and solidification as a function of the turbulent metal flow and the multiple phases present in the caster open the door to prediction of specific problems in the caster such as shell thinning, lack of lubrication and unstable metal level, which are relevant problems in CC in the present day.

REFERENCES

ANAGNOSTOPOULOS, J. and G. BERGELES (1999). "Three-dimensional modeling of the flow and the interface surface in a continuous casting mold model." *Metall. Mater. Trans. B* **30**(6): 1095-1105.

BRACKBILL, J.U., D.B. KOTHE and C. ZEMACH (1992). "A continuum method for modeling surface tension." *J. Comput. Phys.* **100**(2): 335-354.

DAUBY, P.H. (2011). "Real Flows in Continuous Casting Molds." *Iron and Steel Technology* **8**(11): 151-160.

FLUENT-USER-GUIDE (1995-2007). "ANSYS Fluent 6.3.26 - User's Guide." ANSYS Inc.

HASAN, M. and S.H. SEYEDEIN (1998). "3-D numerical prediction of turbulent flow, heat transfer and solidification in a continuous slab caster for steel." *Can. Metall. Q.* **37**(3-4): 213-228.

HIGSON, S.R., P. DRAKE, M. LEWUS, T. LAMP, H. KOCHNER, P. VALENTIN, C. BRUCH, J. CIRIZA, J. LARAUDOGOITIA, J. BJÖRKVALL and L. BERGMAN (2010). "FLOWVIS: measurement, prediction and control of steel flows in the casting nozzle and mould." Final report. RFCS. Luxembourg, European Comission. **EUR 24205**.

HUANG, X. and B.G. THOMAS (1998). "Modeling of transient flow phenomena in continuous casting of steel." *Can. Metall. Q.* **37**(3-4): 197-212.

KUNSTREICH, S. and P.H. DAUBY (2005). "Effect of liquid steel flow pattern on slab quality and the need for dynamic electromagnetic control in the mould." *Ironmak. Steelmak.* **32**(1): 80-86.

LAUNDER, B.E. and D.B. SPALDING (1972). "Lectures in Mathematical Models of Turbulence." London, England., *Cambridge University Press*.

LI, C. and B.G. THOMAS (2002). "Maximum casting speed for continuous cast steel billets based on sub-mold bulging computation." *85th steelmaking Con. Proc.*, Nashville, TN, ISS, Warrendale, PA.

LIOW, J.L., M. RUDMAN and P. LIOVIC (2001). "A volume of fluid (VOF) method for the simulation of metallurgical flows." *ISIJ International* **41**(3): 225-233.

PFEILER, C., M. WU and A. LUDWIG (2005). "Influence of argon gas bubbles and non-metallic inclusions on the flow behavior in steel continuous casting." *Materials science & engineering. A, Structural materials* **413-414**: 115-120.

RAMIREZ-LOPEZ, P.E., P.D. LEE, K.C. MILLS and B. SANTILLANA (2010). "A new approach for modelling slag infiltration and solidification in a continuous casting mould." *ISIJ International* **50**(12): 1797-1804.

RAMIREZ LOPEZ, P.E., P.D. LEE and K.C. MILLS (2010). "Explicit modelling of Slag Infiltration and Shell Formation during Mould Oscillation in Continuous Casting." *ISIJ International* **50**(3): 425-434.

RAMIREZ LOPEZ, P.E., P.D. LEE, K.C. MILLS, C. PUNCREOBUTR, D. FARRUGIA and B. SANTILLANA (2010). "Towards direct defect prediction on continuous casting." *7th European Continuous Casting Conference*, Dusseldorf, Germany.

SANTILLANA, B., B.G. THOMAS, G. BOTMAN and E. DEKKER (2011). "3D thickness measurement technique for continuous casting breakout shells." *7th European Continuous Casting Conference*, Dusseldorf, Germany.

TAKEUCHI, E. and J.K. BRIMACOMBE (1985). "Effect of Oscillation-Mark Formation on the Surface Quality of Continuously Cast Steel Slabs." *Metall. Mater.Trans. B* **16B**(September): 605-625.

THOMAS, B.G. and J.T. PARKMAN (1997). "Simulation of thermal mechanical behaviour during initial solidification." *Thermomechanical Processing of steel and other materials, Thermec*, Australia.

